Parametric study of the vibration-induced repulsion or attraction force on a particle in a viscous fluid cell

Mehrrad Saadatmand*
Mechanical Engineering Department, City College of New York, Convent Avenue at 140th Street, New York, New York 10031, USA

Masahiro Kawaji†
Department of Chemical Engineering and Applied Chemistry, University of Toronto, Toronto, Ontario, Canada M5S 3E5
and Mechanical Engineering Department, City College of New York, Convent Avenue at 140th Street, New York, New York 10031, USA
(Received 30 December 2013; revised manuscript received 8 March 2014; published 9 April 2014)

Experiments and three-dimensional direct numerical simulations were performed to investigate the effects of physical parameters on the repulsion or attraction force affecting the motion of a particle oscillating near a solid wall of a fluid cell under microgravity. The following physical parameters were investigated: fluid cell amplitude, fluid and particle densities, angular frequency of the cell vibration, initial distance between the particle centroid and the closest cell wall, particle radius, and dynamic viscosity. Based on the simulations, a nondimensional relation was developed to relate those physical parameters to the repulsion or attraction force affecting the particle. The relation shows that the repulsion or attraction force is increased by the increase in the cell vibration amplitude and frequency and also the force direction would change from attraction to repulsion above a threshold fluid viscosity. Relations to other physical parameters were also studied and are reported. This paper follows our previous work on the physical mechanism of observed repulsion force on a particle in a viscous fluid cell [M. Saadatmand and M. Kawaji, Phys. Rev. E **88**, 023019 (2013)].

DOI: 10.1103/PhysRevE.89.043009 PACS number(s): 47.10.ad

I. INTRODUCTION

Recent experiments on space platforms have broadened our knowledge of several physical phenomena that have been hidden from our view on earth, due to gravity. One interesting phenomenon observed is the vibration-induced motion of particles in a fluid cell. Under microgravity a particle suspended in a completely liquid-filled fluid cell was expected to remain stationary due to the absence of sedimentation effects and buoyancy-induced convective motion of the fluid. However, the particles in fluid cells on space platforms under microgravity can experience forces due to g-jitter, which occurs on space platforms [1,2]. One example of the effects of g-jitter on the particle motion is the observed movements of protein crystals during their growth in space experiments [3–6]. The g-jitter occurs in random directions with different frequencies, amplitudes, and acceleration levels on space platforms. The sources of g-jitter are mechanical vibrations caused by crew motion; spacecraft maneuvers; operation of different equipment such as pumps, fans, and motors; atmospheric drag; and the earth's gravity gradient [2,7,8]. A comprehensive understanding of this phenomenon could lead to several practical applications, namely, production of crystals of better quality, advanced separation, and agglomeration of particles and droplets.

There are several past studies that investigated the motion of a particle in a fluid starting from Stokes [9], Boussinesq [10], and Basset [11] to the more recent works by Coimbra and Rangel [12] and Hassan and Kawaji [13,14]. Coimbra and Rangel [12] studied the motion of a spherical particle in harmonic Stokes flows and showed that the magnitudes of virtual mass, history, and Stokes drag forces on the particle parallel to the direction of motion are dependent on a scaling number S, defined in terms of the angular vibration frequency, particle radius, and kinematic viscosity of the fluid ($S = \omega R_0^2/9v$). When S is near zero, the Stokes drag is the dominant force on the particle. At $S = 1$, the history drag dominates and when $S > 10^4$ the virtual mass force is the predominant force on the particle.

Recently, Saadatmand *et al.* [15,16] numerically studied the mechanisms of a force acting to attract a particle towards or repulse it from the nearest wall of an inviscid fluid cell in zero gravity. They found that in an inviscid fluid, the attraction force occurs due to the fast motion of the fluid between the particle and the cell wall, which results in a reduction in the fluid pressure in that region. Based on Bernoulli's principle, this reduced pressure in the gap between the particle and the fluid cell wall results in an attraction force towards the wall. In a recent work, Saadatmand and Kawaji [17] showed that in a highly viscous fluid, the fluid velocity between the particle and the wall is reduced. This results in a higher pressure in the gap and net shear stress on the particle, inducing a repulsion force on the particle away from the nearest wall.

The present work is an extended study on the system of a spherical particle in a fluid cell reported in our previous paper [17]. The objective of this study is to clarify the effects of relevant physical parameters on the vibration-induced repulsion or attraction force on a particle in a fluid cell under microgravity. To this end, direct numerical simulations were performed in three dimensions and also experiments and analytical approximations were performed to validate the simulations. To mimic the microgravity environment, the experiments were conducted by suspending a stainless-steel particle by a thin wire in a fluid cell, which was subjected to sinusoidal vibrations of known amplitude and frequency. In the numerical simulation, systematic changes were made in fluid

*msaadatmand@ccny.cuny.edu
†Corresponding author: kawaji@ecf.utoronto.ca

viscosity, particle and fluid densities, particle centroid-to-wall distance, and particle radius. The numerical simulations were validated with the experimental results and a dimensional analysis was performed to derive a nondimensional correlation between the physical parameters and the repulsion or attraction force on the particle induced by the fluid cell vibration.

The simulations in this work were performed using PARTFLOW3D, a direct numerical simulation code developed by Hu *et al.* [18]. The details of the numerical simulation method and code validation were reported in our previous paper [17]. In this paper the experimental details are described first, followed by a dimensional analysis and derivation of a nondimensional correlation.

II. EXPERIMENT

To obtain an environment on the earth for a particle in a fluid cell similar to microgravity, the particle was suspended by a thin wire or a synthetic silk thread from the top of a fluid cell as shown in Fig. 1. Note that Hassan *et al.* [19] already showed that for the cell vibration frequencies above the resonance frequency, the motion of a spherical particle suspended by a thin wire on the ground would correspond to the motion of a wire-free particle in microgravity. The experimental apparatus consisted of a fluid cell mounted on a linear translation stage, a laser confocal displacement sensor to measure the particle motion, another laser displacement sensor, and an accelerometer to monitor the fluid cell vibration.

A. Materials

Two highly viscous fluids were used in the experiments: silicone fluids with kinematic viscosities of 350 and 1000 cSt obtained from Aldrich Chemical Company, Inc. Both fluids were optically clear with a density of 0.97 g/cm^3 at room temperature. For some of the experiments, deionized water obtained from a reverse osmosis system was also used as a nearly inviscid fluid. The deionized water was degassed by boiling for half an hour and cooled down before it was placed in the fluid cell.

Particle and wire. Two spherical balls (12.7 and 4.0 mm in diameter) made of stainless steel ($\rho_p = 7.9$ g/cm^3) were used as the particles. The 12.7-mm-diam particle was attached to a thin metal wire by soldering. For the 4.0-mm-diam particle, a hole of 1.0 mm diameter was drilled all the way through the ball and a synthetic silk thread of 30 μm diameter was attached to the particle by knotting it to a pin and inserting the pin into the hole. Both particles were hung from the ceiling of the fluid cell. The wire used for suspending the 12.7-mm particle was Alomega® wire from Omega Engineering, Inc. The wire diameter was 25 μm (the smallest diameter available) to minimize the drag force of the surrounding viscous fluid on the wire. Only for the experiments conducted with water was a 125-μm-diam wire used. Note that Hassan *et al.* [20] found that wire diameters equal to or less than 125 μm would not exert any influence on the vibration-induced particle oscillation amplitude in a water-filled fluid cell. All the components of the experimental apparatus were installed on a vibration-isolating optical table to be isolated from external sources of vibration.

B. Design of the fluid cell

The experimental apparatus consisted of a rectangular fluid cell mounted on a computer-controlled linear translation stage (Fig. 1). The fluid cell was made of smooth, polished acrylic plates of 10 mm thickness with internal dimensions of 140-mm height and (50 × 50)-mm cross section.

Linear translation stage. A translation stage controlled by a computer was used to produce horizontal sinusoidal vibrations. The translation stage was a linear positioner from Parker-Daedal Corporation. The amplitude and frequency of the cell vibration were controlled by a PC equipped with Motion Architect software. The translation stage was capable of producing submicron resolution vibrations with sufficient repeatability.

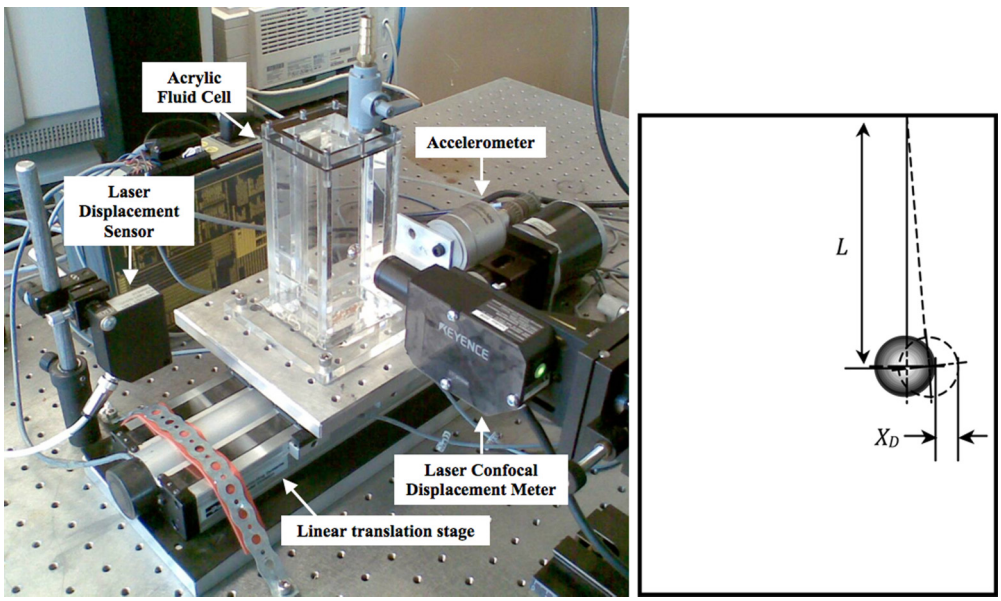

FIG. 1. (Color online) Experimental setup and side view of the fluid cell.

Laser displacement meters. A laser confocal displacement sensor [LT-9030 (M) from Keyence Canada, Inc.] was used to measure the particle motion (Fig. 1). The laser sensor's resolution was 0.1 μm. Moreover, the laser sensor was equipped with an internal microscope with 44 $\times$ magnification. A second laser displacement sensor (OptoNCDT 1401-5 from Micro-Epsilon) was used to measure the exact position of the translation stage. The sensor had a resolution of 3.0 μm for dynamic objects at 1 kHz. The signal from the second laser displacement sensor was used to plot the translation stage movement versus time and to find the actual frequency and amplitude of the cell vibrations.

Accelerometer. An accelerometer (from Dytran Instruments, Inc., model No. 3191A1) was used to directly measure the acceleration of the fluid cell on the translation stage and also the background vibration during the experiments. The measurement range for the accelerometer was from $-0.5g$ to $0.5g$ with $7 \times 10^{-6}g$ resolution (where $1g$ is normal gravity) (Fig. 1).

C. Procedure

Unless otherwise stated, in all the experiments, the length of the wire or synthetic silk thread was adjusted to fix the vertical distance between the fluid cell ceiling and the center of the particle at 76.0 mm. The distance from the edge of the particle to the nearest cell wall δ before the start of the cell vibrations was 0.85 mm for silicone fluids and 0.82 mm for water.

Figure 2 shows a top view of the particle in the fluid cell. The particle was positioned at equal distances from the cell walls 2 and 4 and the vibration of the fluid cell was parallel to the cell walls 1 and 3. The vibration frequency and amplitude of the fluid cell were controlled by the linear translation stage. The fluid cell was subjected to sinusoidal vibrations from 0.25 to 15 Hz in frequency. In each set of experiments, the cell vibration amplitude was kept constant. Overall, the experiments were conducted with three different cell vibration amplitudes of 0.50, 0.75, and 1.0 mm. Each set of experiments was repeated at least three times to ensure the reproducibility of the data.

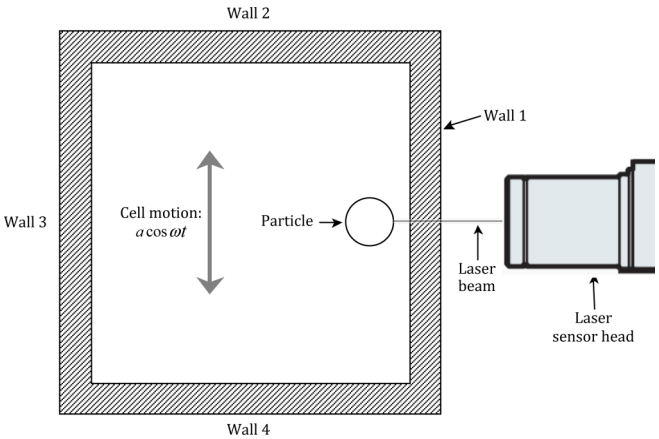

FIG. 2. (Color online) Top view of the fluid cell with the cell walls labeled.

Measuring the movement of the particle was performed by the laser confocal displacement sensor. The transparency of both the acrylic cell walls and fluid allowed easy tracking of the particle's displacement in the direction perpendicular to the cell wall 1. The data from the laser confocal displacement sensor were recorded by the data acquisition system and analyzed to determine the particle displacement. The procedure for each experimental run consisted of three consecutive steps: keeping the fluid cell motionless for 100 s, followed by vibration of the cell for another 100 s, and finally keeping the cell motionless for the final 100 s. During the cell vibration, the plane of particle oscillation shifted away from (repulsion) or towards (attraction) the nearest cell wall 1.

III. NUMERICAL SIMULATIONS

The numerical simulation code used in this work is PARTFLOW3D, which was developed by Hu *et al.* [18]. The code is a direct numerical simulation without simplifying assumptions. The code can perform three-dimensional simulations of the motion of solid particles in a fluid cell. A description of the code taken from Hu *et al.* [18] is summarized below. A finite-element technique has been used in this code, which solves the equations of motion for both the fluid and particle combined into a single equation of motion. An arbitrary Lagrangian-Eulerian technique is used in this code, which utilizes the standard Galerkin finite-element method. The positions of the particle and mesh are updated explicitly at each time step and the velocities of the fluid and the particle are calculated implicitly. The governing equations in this code are the conservation of mass and momentum for the fluid motion, the Euler equations for the particle rotation, and Newton's second law for the translational motion of the particle.

For this study PARTFLOW3D predicted the motion of a particle in a sinusoidally vibrated fluid cell in a fixed frame of reference. The cell acceleration was specified through the body force $\mathbf{f}$ defined as

$$\mathbf{f} = \mathbf{g}_s - A_c\omega^2 \sin(\omega t), \tag{1}$$

where $\mathbf{g}_s$ is a steady residual acceleration (assumed to be zero here), A_c is the cell vibration amplitude (half of the peak-to-peak amplitude), and ω is the angular frequency ($=2\pi f$). The nonslip boundary condition on the particle surface was

$$\mathbf{u} = \mathbf{V}_i + \boldsymbol{\omega}_i \times (\mathbf{x} - \mathbf{X}_i), \tag{2}$$

where $\mathbf{u}$ is the velocity of fluid, $\mathbf{V}_i$ is the velocity of particle, $\boldsymbol{\omega}_i$ is the angular velocity of the particle, $\mathbf{X}_i$ is position of the sphere centroid, and $\mathbf{x}$ is the position of a given point on the particle surface. For the boundaries of the computational domain, cell walls, the nonslip boundary condition was

$$\mathbf{u} = \mathbf{0}. \tag{3}$$

Hu *et al.* [18] derived a weak formulation to use the finite-element method, which incorporated both the fluid and particle equations of motion. The formulation was derived by multiplying the momentum equation by a test function for the fluid velocity $\tilde{\mathbf{u}}$ and integrating at time t over the fluid domain. For the particles, this test function would be replaced by Eq. (2). The combined fluid-particle momentum equation

would have the form

$$\int_{\Omega_0} \rho_f \left(\frac{D\mathbf{u}}{Dt} - \mathbf{f}\right) \cdot \tilde{\mathbf{u}} d\Omega + \int_{\Omega_0} \sigma : \mathbf{D}[\tilde{\mathbf{u}}] d\Omega + \sum_{1 \leqslant i \leqslant N} \tilde{\mathbf{V}}_i \cdot \left(m_i \frac{d\mathbf{V}_i}{dt} - \mathbf{G}_i\right) + \sum_{1 \leqslant i \leqslant N} \tilde{\omega}_i \cdot \frac{d(\mathbf{I}_i \omega_i)}{dt} = 0, \tag{4}$$

where ρ_f is the fluid density, Ω is the computational domain, σ is the stress tensor, m_i is the mass, $\mathbf{V}_i$ is the translational velocity of the ith particle, $\mathbf{G}_i$ is the external body force, and $\mathbf{I}_i$ is the moment of inertia matrix. This equation considers the fluid and particles as one system and therefore the forces related to the fluid turn to internal forces in the formulation. That is why the forces and moments acting on the particle do not explicitly appear in the formulation. Combining the momentum equations of the fluid and particle reduces the computational time substantially.

This code was validated in our previous paper [17] using Tchen's [21] equation and also has been compared with experimental data [22]. Moreover, as Figs. 6 and 7 show, the numerical predictions of this code are in good agreement with the experimental data.

IV. RESULTS AND DISCUSSION

A. Experimental results

The goal of the experiments was to determine the response of the particle to small horizontal vibrations in a viscous fluid cell. Specifically, it was desired to assess whether such a particle would experience a vibration-induced attraction or repulsion force from the nearest wall of the fluid cell.

Unlike the attraction force observed in an inviscid fluid cell by Hassan *et al.* [20] and also observed in the present experiments conducted with a water-filled cell, a repulsion force was observed for a 4.0-mm stainless-steel ball in a viscous fluid cell as shown in Fig. 3, pushing the plane of the oscillating particle away from the nearest wall in all the experiments at frequencies higher than 6.0 Hz. In this figure the repulsion force is indicated by negative particle displacements and attraction force by positive displacements from the neutral position, which is the position of the particle at rest where the displacement is zero. The displacement of the 4.0-mm-diam particle from the neutral position increased in magnitude with the cell vibration amplitude and frequency due to an increased repulsion force, except for the smallest cell amplitude of 0.5 mm. Larger cell amplitudes of 0.75 and 1.0 mm always resulted in a repulsion force acting on the particle. A complete set of experimental results is reported by Saadatmand [22].

Saadatmand and Kawaji [23] previously investigated the repulsion force exerted on a 12.7-mm-diam stainless-steel particle suspended in 350- and 1000-cSt silicone fluid-filled cells subjected to sinusoidal vibrations. They reported three main observations: (i) a repulsion force on the particle for cell amplitudes of 0.50–1.00 mm and frequencies higher than 5 Hz, (ii) an increase of the repulsion force with increasing fluid viscosity, and (iii) an increase in the repulsion force by increasing both frequency and amplitude of the cell vibrations.

As Fig. 3 shows, the drift in the plane of the particle oscillation from the nearest cell wall is greater for larger cell vibration amplitudes as the repulsion force increases with the cell vibration amplitude for a given vibration frequency. Moreover, an increase in the vibration frequency results in a higher repulsion force on the particle. Similar results were previously found by Hassan *et al.* [19] but for an attraction force in an inviscid fluid. They showed that the attraction force and also the particle drift for an inviscid fluid are proportional to the square of both the cell vibration amplitude and frequency.

Figure 4 shows the particle amplitude varying with the cell amplitude for a 4.0-mm-diam particle. For each vibration frequency, the particle amplitude is seen to vary linearly with the cell amplitude.

B. Comparison of simulation results with experimental data

In this section the PARTFLOW3D code predictions are compared with some of the experimental results. The complete comparison is reported elsewhere [22]. It is important to note

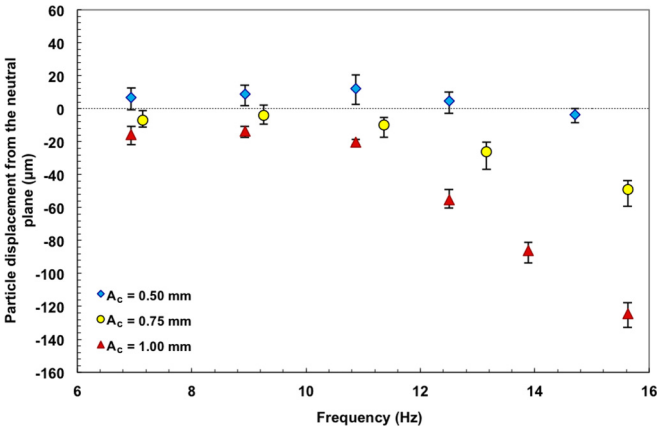

FIG. 3. (Color online) Transverse particle displacement from a neutral position as a function of cell frequency and amplitude for 1000-cSt silicone oil and a steel particle of 4.0 mm diameter suspended by a synthetic silk thread. For all cases δ was 0.85 mm.

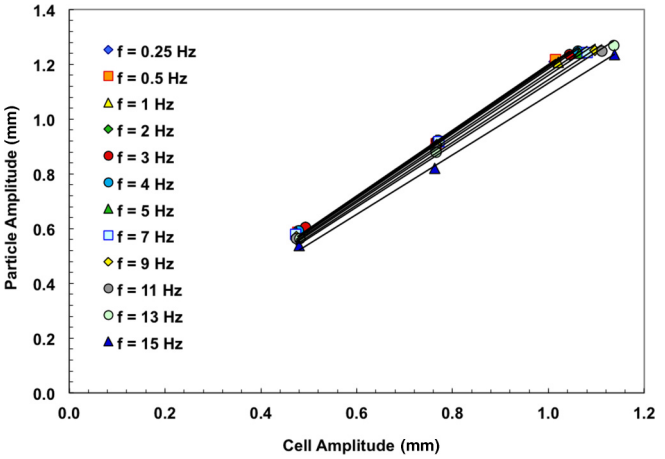

FIG. 4. (Color online) Variation of particle amplitude with cell amplitude for 1000-cSt fluid and three different cell amplitudes (with a particle diameter of 4.0 mm, synthetic silk thread, and $\delta = 0.85$ mm).

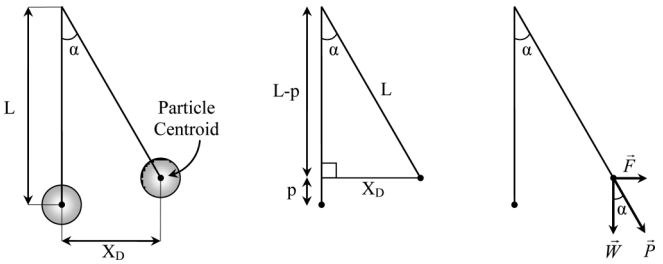

FIG. 5. Force balance around the particle.

that the simulations performed with PARTFLOW3D are only related to a wire-free particle in microgravity environment, while the experiments have been conducted under normal gravity by suspending a particle in the fluid cell by a thin wire or thread. Therefore, a perfect match between the experiments and simulations cannot be expected and the main objective here is to understand the behavior of a wire-free particle in microgravity and compare it with the experimental results obtained on the ground.

To obtain the repulsion or attraction force exerted on a particle near the cell wall from the experiments, the displacement of the plane of particle oscillation from its neutral position X_D was used to calculate the repulsion force. During each experiment, the plane of the particle oscillation shifted from its neutral position by X_D and the average position of the particle on the axis normal to the wall could be determined. Therefore, it was possible to use a simple force balance as illustrated in Fig. 5 to calculate the repulsion or attraction force exerted on the particle

$$F = \frac{4}{3}\pi(\rho_p - \rho_f)gR_0^3\frac{X_D}{\sqrt{L^2 - X_D^2}}. \quad (5)$$

To simulate the motion of a particle suspended by a wire using the PARTFLOW3D code, the plane of the particle oscillation was fixed in the y direction normal to the nearest cell wall. This prevented the particle from moving towards or away from the nearest wall and made the scenario similar to a wire-suspended particle in the experiments. However, the motion of the particle parallel to the wall was the same as that of a wire-free particle in microgravity.

Figures 6 and 7 show that the simulations can well predict the attraction or repulsion of the particle towards the wall depending on the fluid viscosity. Small differences observed between the experimental data and numerical results in these figures can be attributed to the effects of particle suspension and gravity. While the simulations were conducted for a wire-free particle in zero gravity, the experiments were performed under normal gravity using a thin thread or wire to suspend the particle. Gravity acting on the suspended particle would always pull the particle downward so that the particle's oscillation amplitude would be reduced slightly under normal gravity. So, for water with low viscosity, smaller particle amplitudes and thus smaller attraction forces would be expected in the present experiments compared to the numerical simulations as shown in Fig. 6. This would also be true for the repulsion forces shown in Fig. 7, which are much smaller in magnitude than the attraction forces shown in Fig. 6 due to the much smaller particle amplitude in a highly viscous fluid surrounding the particle.

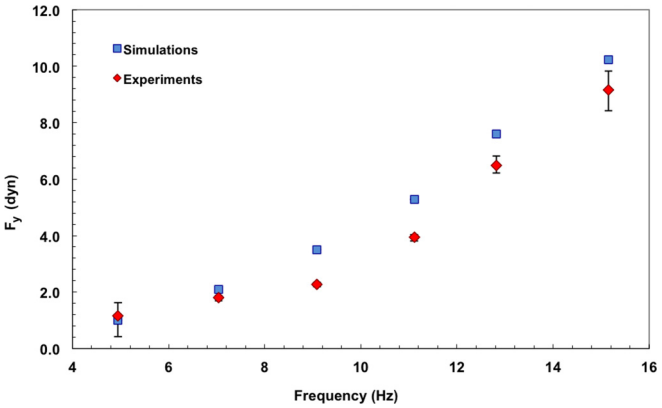

FIG. 6. (Color online) Attraction force as a function of cell frequency obtained from experiments and simulations for a steel particle of 12.7 mm diameter suspended in water ($\delta = 0.82$ mm).

Another difference to note between the experiment and numerical simulation is the trajectory of the particle during each oscillation. In the numerical simulations, the plane of the particle oscillation was fixed regardless of the attraction or repulsion force arising from the oscillation. However, in the experiments, the vibration-induced attraction or repulsion force would pull or push the particle in the direction normal to the nearest wall, so the particle trajectory in a given oscillation cycle would not remain perfectly parallel to the nearest wall. Thus, we cannot expect perfect agreement between the experimental and simulation results presented in Figs. 6 and 7.

C. Repulsion or attraction force on a constrained particle near a fluid cell wall

The repulsion or attraction force on a particle oscillating near a fluid cell wall is essentially the result of nonuniform pressure distributions and shear stresses around the particle moving inside a fluid of different density. In a fluid cell completely filled with a liquid under microgravity environment, the

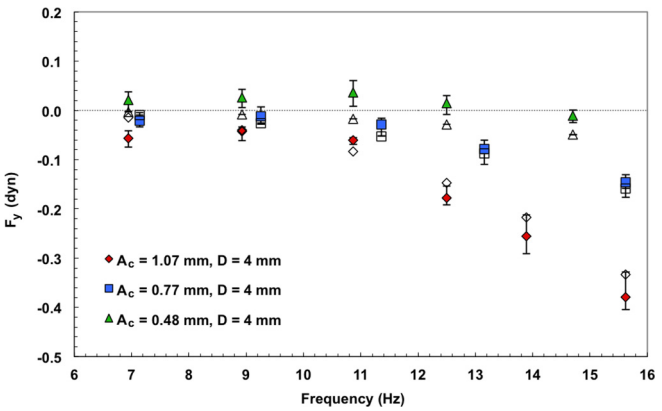

FIG. 7. (Color online) Repulsion force as a function of cell frequency obtained from experiments (closed symbols) and simulations (open symbols) for a steel particle of 4.0 mm diameter suspended in 1000-cSt silicone oil ($\delta = 0.85$ mm).

TABLE I. Parameters affecting a particle near a fluid cell wall.

Quantity	Symbol	Dimensions (M,L,T)	Range used for Eq. (15)
repulsion or attraction force	F_y	MLT^{-2}	
cell amplitude	A_c	L	0.0–0.552 cm
cell angular frequency	ω	T^{-1}	0.006–221.6 rad/s
liquid density	ρ_f	ML^{-3}	0.0–10.0 g/cm^3
particle density	ρ_p	ML^{-3}	1.0–21.45 g/cm^3
particle radius	R_0	L	0.01–0.5 cm
distance from particle centroid to the wall	H	L	0.21–2.5 cm[a]
dynamic viscosity	μ	$ML^{-1}T^{-1}$	0.01–100 g/cm s

[a]The particle radius for this range was 0.2 cm.

TABLE II. Parameters used for the base case of the simulations.

Parameter	Value	Remarks
cell amplitude A_c (cm)	0.2	
cell frequency f (Hz)	10	
fluid density ρ_f (g/cm^3)	1	density of water
particle density ρ_p (g/cm^3)	7.9	density of steel
particle radius R_0 (cm)	0.2	
initial distance from particle centroid to the nearest cell wall H (cm)	0.21	
dynamic viscosity μ (g/cm s)	0.01	viscosity of water
cell size $x \times y \times z$ (cm^3)	$14 \times 5 \times 5$	
particle initial position x (cm)	7.6	nearly half cell size
particle initial position y (cm)	4.79	cell side $-H_0$
particle initial position z (cm)	2.5	half cell size

fluid motion directly affects the particle motion by producing different pressure distributions, shear forces, and also vortices around the particle. Several physical parameters control the movement of the particle. Among them eight parameters are of importance, as listed in Table I.

Based on the number of parameters $n = 8$ and $m = 3$ dimensions, five dimensionless groups can be obtained:

$$n - m = 8 - 3 = 5. \tag{6}$$

Using the repeating variables ω, ρ_f, and R_0, the dimensionless groups were found as

$$\Pi_1 = \frac{F}{\rho_f \omega^2 R_0^4} = \tilde{F}, \tag{7}$$

$$\Pi_2 = \frac{A_c}{R_0} = \tilde{A}_c, \tag{8}$$

$$\Pi_3 = \frac{\rho_f}{\rho_p} = \tilde{\rho}, \tag{9}$$

$$\Pi_4 = \frac{H}{R_0} = \tilde{H}, \tag{10}$$

$$\Pi_5 = \frac{\rho_f \omega R_0^2}{\mu} = \tilde{S}. \tag{11}$$

Equations (7)–(11) suggest that $\tilde{F} = f(\tilde{A}_c, \tilde{\rho}, \tilde{H}, \tilde{S})$. These dimensionless groups were used to study the effects of different physical parameters of the system on the repulsion or attraction force affecting the particle motion.

To investigate the effects of changing the physical parameters on the repulsion or attraction force, direct numerical simulations were conducted using PARTFLOW3D. All the simulations presented in this paper are for a particle oscillating sinusoidally in the x-z plane parallel to the closest cell wall. In order to find a net average force on the particle in the y axis perpendicular to the closest wall, the plane of the particle oscillation was fixed at a certain distance on the y axis. This technique was used due to the fact that under microgravity after the start of the vibrations of the fluid cell, a free particle oscillating in the cell would drift away from its original position. This drift would be either towards or away from the closest cell wall. Since the repulsion or attraction force would noticeably vary with the particle position, the predicted forces would also change for quasisteady particle oscillation if the particle is allowed to oscillate and move towards or away from the wall.

To better compare the simulation results, a base case was considered for the simulations of this section. Table II shows the base case parameter values. In order to check the effect of each physical parameter, only that parameter was varied in most cases over the range shown in Table I. The simulations of this section were conducted using a fluid cell of $14 \times 5 \times 5$ cm^3 and a steel particle of 4.0 mm diameter. The fluid for the base case had the same properties as water at room temperature. The mesh density for the background flow was varied from 64 000 to 343 000 and increased in the region around the particle. It was confirmed that a further increase in the mesh density beyond 343 000 would not change the predicted results by more than 1%.

In the following figures, all the available experimental data are shown along with the numerical simulation results.

1. Cell amplitude

Ten simulations were conducted to ascertain the relation between the cell amplitude and the net repulsion or attraction force on the particle in the direction perpendicular to the closest cell wall. In these simulations the dimensionless cell amplitude $\tilde{A}_c$ was varied from 0.275 to 2.76 with corresponding Reynolds numbers of 101 to 1068 ($\mathrm{Re} = 2\rho_f A_p \omega R_0/\mu$). In this set of simulations two parameters were different from the base case: $H_0 = 0.4$ cm and $y = 4.6$ cm. A simple analysis of the results showed that the repulsion or attraction force $\tilde{F}_y$ along the y axis perpendicular to the nearest cell wall is proportional to the second power of the cell amplitude (Fig. 8)

$$\tilde{F}_y \propto \tilde{A}_c^2. \tag{12}$$

2. Fluid and particle densities

To investigate the effects of the fluid and particle densities, nine simulations were conducted with different fluid densities as well as ten simulations with different particle densities. The first set of simulations was conducted by setting $\rho_p = 10.0$ g/cm^3 and changing ρ_f from 0.45 to 10.0 g/cm^3 so $\tilde{\rho}$ ranged from 0.045 to 1.0. In the second set, $\tilde{\rho}$ was changed from 1.0 to 0.05 by changing the particle density

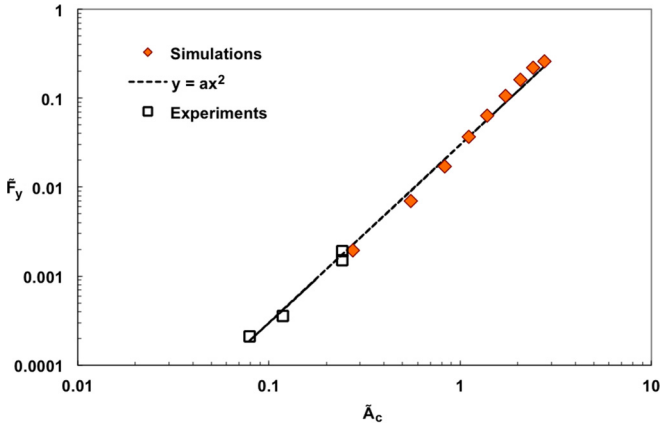

FIG. 8. (Color online) Dimensionless attraction force as a function of dimensionless cell amplitude; the slope of the line is 2.0.

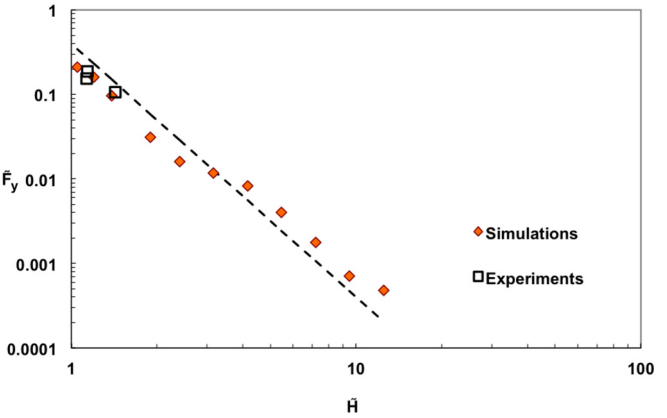

FIG. 10. (Color online) Dimensionless attraction force as a function of $\tilde{H}$; the slope of the dashed line is −3.0.

from 1.0 to 21.45 g/cm^3 and the Reynolds number from 87 to 835. The simulation results suggest the following relation between the dimensionless repulsion or attraction force and the dimensionless density ratio (Fig. 9):

$$\tilde{F}_y \propto \left(\frac{1-\tilde{\rho}}{2+\tilde{\rho}}\right)^2. \tag{13}$$

3. Initial distance between the particle centroid and nearest cell wall

The relation between the position of the plane of particle oscillation and the repulsion or attraction force is probably the most interesting one. In the simulations, the distance between the particle centroid and the nearest cell wall $\tilde{H}$ was changed from 1.05 to 12.50, with the latter value corresponding to the particle at the center of the fluid cell. Due to the same physical parameters used in these simulations, the Reynolds number was almost the same for all the simulations (∼350). Moreover, the predicted particle amplitudes were very close for all cases. Although the Reynolds number was nearly equal for different values of $\tilde{H}$, the simulations revealed that decreasing the particle centroid to the nearest wall distance $\tilde{H}$ sharply increases the attraction or repulsion force. This physically means that the same acceleration of the fluid cell can lead to dramatically different repulsion or attraction force on the particle depending on the particle centroid to the nearest wall distance. Furthermore, the simulations also reveal that there is an almost linear relation between the repulsion or attraction force and $\tilde{H}$ in a logarithmic plot (Fig. 10). These results suggest the following relation for the repulsion or attraction force as a function of $\tilde{H}$:

$$\tilde{F}_y \propto \tilde{H}^{-3}. \tag{14}$$

4. Scaling parameter $\tilde{S}$

The effects of fluid viscosity on the repulsion or attraction force acting on the particle were studied by conducting 24 simulations with different fluid viscosities. The scaling parameter $\tilde{S} = \rho_f \omega R_0^2/\mu$ given by Eq. (11) was used for this purpose and varied in these simulations from 0.025 to 251.3. Note that the scaling parameter $\tilde{S}$ is proportional to the scaling number S, defined by Coimbra and Rangel [12] ($\tilde{S} = S/9$). Based on the changes in $\tilde{S}$, the Reynolds number varied from 0.000 74 for $\tilde{S} = 0.025$ to 357.8 for $\tilde{S} = 251.3$. Figure 11 shows the repulsion or attraction force as a function of $\tilde{S}$. As it can be seen, the increase in the viscosity of the fluid has a profound effect on the force. The attraction force increases at low viscosities ($\tilde{S} > 43.5$) and its sign changes to repulsion as

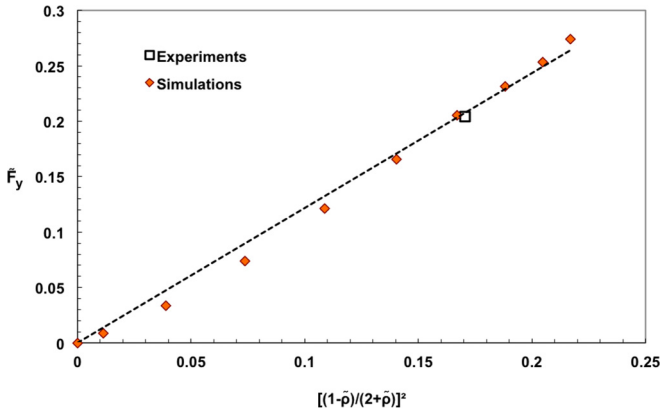

FIG. 9. (Color online) Attraction force as a function of $[(1-\tilde{\rho})/(2+\tilde{\rho})]^2$ for the change in the solid density.

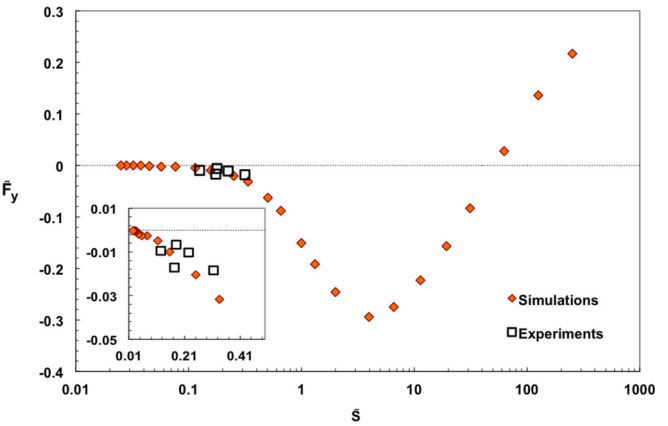

FIG. 11. (Color online) Dimensionless attraction or repulsion force as a function of $\tilde{S} = \rho_f \omega R_0^2/\mu$.

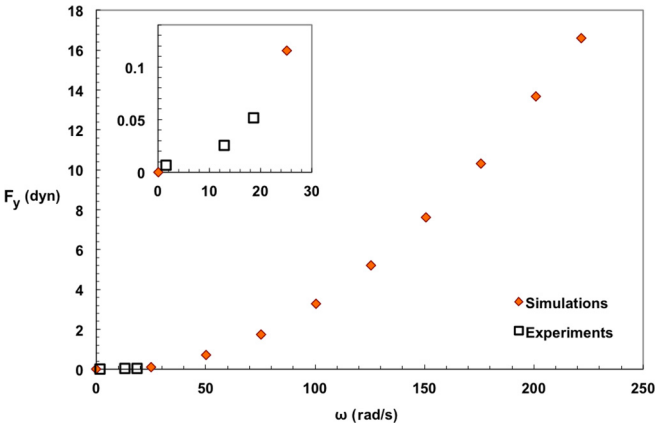

FIG. 12. (Color online) Attraction force as a function of dimensionless cell frequency.

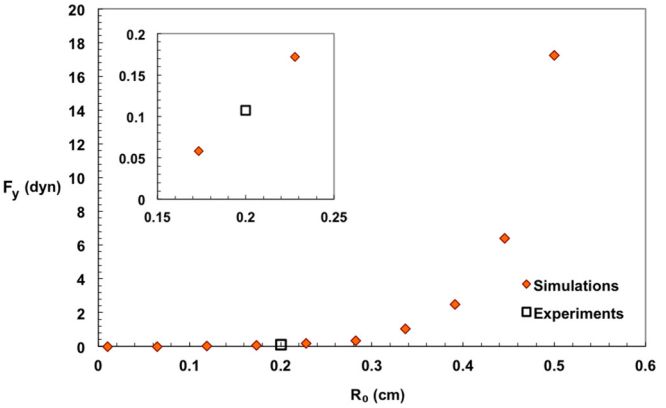

FIG. 13. (Color online) Attraction force as a function of particle radius.

the fluid viscosity increases ($\tilde{S} < 43.5$). At $\tilde{S} \approx 4$ the repulsion force has a maximum magnitude and then it starts to decrease to zero for higher viscosities or lower $\tilde{S}$. Around $\tilde{S} \approx 0.1$ the force reaches nearly zero and does not change by a further increase in the viscosity or decrease in $\tilde{S}$.

While the scaling parameter has been studied here as a nondimensional parameter representing the viscosity, it is proportional to the angular vibration frequency, fluid density, and the square of the particle radius. Since the effects of fluid and particle densities were discussed in the previous section it would be informative to also discuss the relation between the repulsion or attraction force and the angular frequency of cell vibration and particle radius here.

The relation between the cell vibration frequency ω and the net repulsion or attraction force was investigated by conducting ten simulations. In this set of simulations, ω was varied from 0.0063 to 221.6, corresponding to a range of Reynolds numbers from $\mathrm{Re} = 9.6 \times 10^{-4}$ to 1300. Moreover, two parameters were different from the base case: $H = 0.23$ cm and $y = 4.77$ cm. The results of these simulations reveal that the attraction force increases with an increase in the cell angular frequency (Fig. 12). This is reasonable since the particle velocity is proportional to the cell angular frequency.

Next, to ascertain the effects of a change in the particle radius on the repulsion or attraction force, ten simulations were conducted. The particle radius was varied from 0.01 to 0.50 cm. To accommodate these changes, H_0 and y were also varied from the base case to 0.51 and 4.49 cm, respectively. The simulation results show a change in Reynolds number from 9.7 to 830 for the smallest to largest R_0 and that the attraction force substantially increases with the particle radius (Fig. 13).

5. *Collapse of the data*

Performing direct numerical simulations using PARTFLOW3D has proved to be highly useful for predicting the behavior of the particle in a fluid cell under a specific physical situation. However, finding a semiempirical equation can help in understanding the parametric effects and also the relative importance of each physical parameter in the behavior of the particle. By studying the simulation results for all cases, the following nondimensional relation could be derived:

$$\tilde{F}_y = \frac{\tilde{A}_c^2}{\tilde{H}^3}\left(\frac{1-\tilde{\rho}}{2+\tilde{\rho}}\right)^2\left[\frac{5.333\tilde{S}}{34.526+\tilde{S}} - 3.210e^{-1/\tilde{S}}\right]. \quad (15)$$

Figure 14 shows a plot of Eq. (15). The ranges of dimensionless parameters covered by this relation are given in Table III. This relation should be used with care, as it is valid only for the specified ranges of the parameters investigated here. Nevertheless, for studying the repulsion or attraction force on a particle in a viscous fluid cell, Eq. (15) would provide a good estimate without performing additional numerical simulations.

Equation (15) shows that the repulsion or attraction force on a particle oscillating parallel to the closest cell wall increases with the second power of the cell amplitude and the cell vibration frequency. Moreover, the distance $\tilde{H}$ between the particle centroid and the nearest cell wall has a negative

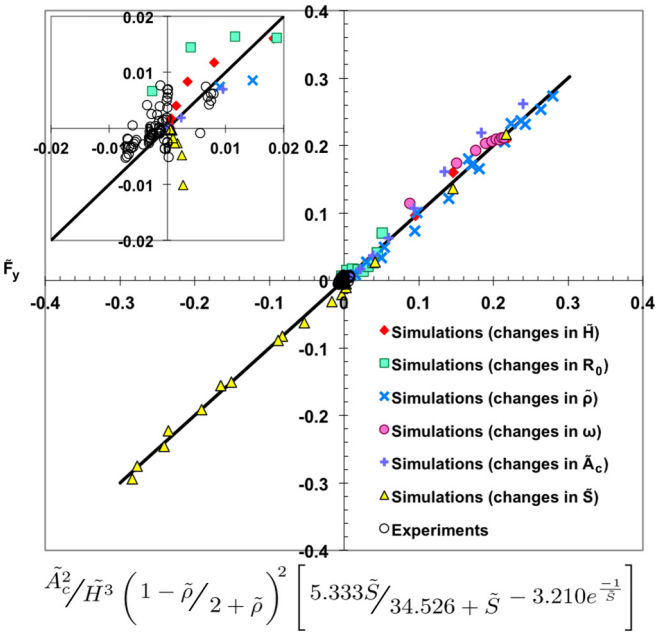

FIG. 14. (Color online) Comparison of predicted repulsion or attraction force, Fy, in symbols with Eq. (15) shown by a solid line.

TABLE III. Range of dimensionless parameters used in Eq. (15).

Dimensionless quantity	Symbol	Range used for Eq. (15)
cell amplitude	$\tilde{A}_c$	0.275–2.76
distance from particle centroid to the wall	$\tilde{H}$	1.05–12.50
density	$\tilde{\rho}$	0.045–1.0
scaling parameter	$\tilde{S}$	0.025–251.3

exponent −3.0. This means that changing this parameter even slightly can dramatically affect the repulsion or attraction force on the particle. The closer the particle is to the cell wall, the greater the magnitude of the repulsion or attraction force would be. The relation between the force and particle and fluid densities is more complicated. However, as Eq. (15) shows quite logically, if the particle and the fluid densities are equal as in a neutrally buoyant system, the repulsion or attraction force would be zero. Moreover, increasing the particle density to very high values ($\tilde{\rho} \to \infty$) will lead to a limiting value of the density term in Eq. (15) as follows:

$$\lim_{\tilde{\rho}\to\infty}\left(\frac{1-\tilde{\rho}}{2+\tilde{\rho}}\right)^2 = \frac{1}{4}. \tag{16}$$

Thus, if the particle is sufficiently heavy, its density will no longer affect the repulsion or attraction force. Another implication of Eq. (15) is that if the particle density is kept constant but the fluid density is changed, there would be a fluid density that maximizes the magnitude of the density term in Eq. (15) and therefore the magnitude of the repulsion or attraction force

$$\rho_f = \left(\frac{\sqrt{57}-7}{2}\right)\rho_p = 0.275\rho_p. \tag{17}$$

Thus, the net repulsion or attraction force would be maximized when the particle is about 3.6 times denser than the liquid.

The last term on the right hand side of Eq. (15) describes the contribution of the viscosity to the repulsion or attraction force. The term $5.333\tilde{S}/(34.526+\tilde{S})$ accounts for the attraction force on the particle towards the wall and the term $-3.210e^{-1/\tilde{S}}$ is related to the repulsion force. When $\tilde{S} = 49.6$ these two terms are almost equal and the net force approaches zero. Below this value the force would be repulsive and above this value the force would be attractive.

V. CONCLUSION

The effects of different physical parameters on vibration-induced attraction or repulsion force affecting an oscillating particle in a fluid cell were studied experimentally and by conducting direct numerical simulations in three dimensions. The simulation results were in good agreement with the experimental results and both showed the existence of a repulsion or attraction force in the fluid cell displacing the plane of the oscillating particle away from or towards the nearest wall of the fluid cell. The displacement of the particle from its rest position was increased in magnitude by the increase in the cell vibration amplitude and frequency due to an increased repulsion or attraction force on the particle. The repulsion or attraction force obtained from the simulation results could be correlated in terms of a combination of all the parameters as given by Eq. (15). This nondimensional correlation shows that the force on the particle is increased sharply by the decrease in the distance between the particle centroid and the nearest cell wall. Moreover, the direction of the force changes from repulsion to attraction by the increase in the scaling parameter $\tilde{S}$ above a threshold value.

The present study reveals a method, based on small vibrations of a fluid cell, to manipulate a particle and possibly a group of small particles in fluids. The phenomenon studied could possibly be used in selective separation or agglomeration of small particles in fluid cells based on their physical parameters. Many different applications related to systems of small particles and fluids could be developed by further studying the vibration-induced repulsion or attraction force.

ACKNOWLEDGMENTS

The authors would like to thank the Canadian Space Agency for an SSEP grant to financially support this work. We would also like to thank Professor Howard H. Hu at University of Pennsylvania for providing the PARTFLOW3D code and helping us in the use of this code.

[1] S. Ostrach, Annu. Rev. Fluid Mech. **14**, 313 (1982).
[2] W. Knabe and D. Eilers, Acta Astronaut. **9**, 187 (1982).
[3] N. E. Chayen, E. H. Snell, J. R. Helliwell, and P. F. Zagalsky, J. Cryst. Growth **171**, 219 (1997).
[4] B. Lorber, J. D. Ng, P. Lautenschlager, and R. Giege, J. Cryst. Growth **208**, 665 (2000).
[5] M. Kawaji, O. Gamache, D. H. Hwang, N. Ichikawa, J. P. Viola, and J. Sygusch, J. Cryst. Growth **258**, 420 (2003).
[6] S. Simic-Stefani, M. Kawaji, and H. H. Hu, J. Cryst. Growth **294**, 373 (2006).
[7] K. Jules, K. McPherson, K. Hrovat, E. Kelly, and T. Reckart, Acta Astronaut. **55**, 335 (2004).
[8] S. Shafie, N. Amin, and I. Pop, Mech. Res. Commun. **34**, 115 (2007).
[9] G. G. Stokes, Trans. Cambridge Philos. Soc. **9**, 8 (1851).
[10] J. Boussinesq, C. R. Acad. Sci. Paris **100**, 935 (1885).
[11] B. Basset, *A Treatise on Hydrodynamics* (Deighton, Bell and Co., Cambridge, UK, 1888), Chap. 21, pp. 260–284.
[12] F. M. Coimbra and R. H. Rangel, AIAA J. **39**, 1673 (2001).
[13] S. Hassan and M. Kawaji, AIAA J. **45**, 2090 (2007).
[14] S. Hassan and M. Kawaji, Microgravity Sci. Technol. **19**, 109 (2007).
[15] M. Saadatmand, M. Kawaji, and H. H. Hu, *Proceedings of the Seventh International Conference on Multiphase Flow, ICMF 2010, Tampa* (University of Florida, Gainesville, 2010).

[16] M. Saadatmand, M. Kawaji, and H. H. Hu, Microgravity Sci. Technol. **24**, 53 (2012).
[17] M. Saadatmand and M. Kawaji, Phys. Rev. E **88**, 023019 (2013).
[18] H. H. Hu, N. A. Patankar, and M. Y. Zhu, J. Comput. Phys. **169**, 427 (2001).
[19] S. Hassan, M. Kawaji, T. P. Lyubimova, and D. V. Lyubimov, J. Appl. Mech. **73**, 610 (2006).
[20] S. Hassan, T. P. Lyubimova, D. V. Lyubimov, and M. Kawaji, Int. J. Multiphase Flow **32**, 1037 (2006).
[21] C. M. Tchen, Ph.D. Thesis, Delft University of Technology, 1947.
[22] M. Saadatmand, Ph.D. thesis, University of Toronto, 2012.
[23] M. Saadatmand and M. Kawaji, Microgravity Sci. Technol. **22**, 433 (2010).